Proceedings of GPPS Forum 18
Global Power and Propulsion Society
Montreal, 7th-9th May 2018
www.gpps.global

GPPS-2018-0026

Electrically driven, Compact, Transonic Mixed-Flow Compressor for Active High-Lift Systems in Future Aircraft

Felix Kauth
Institute of Turbomachinery and Fluid Dynamics
Leibniz Universität Hannover
Kauth@tfd.uni-hannover.de
Hannover, Germany

Gerrit Narjes
Institute for Drive Systems and Power Electronics
Leibniz Universität Hannover
Gerrit.narjes@ial.uni-hannover.de
Hannover, Germany

Jan-Kaspar Müller
Institute for Drive Systems and Power Electronics
Leibniz Universität Hannover
Jan.mueller@ial.uni-hannover.de
Hannover, Germany

Axel Mertens
Institute for Drive Systems and Power Electronics
Leibniz Universität Hannover
Mertens@ial.uni-hannover.de
Hannover, Germany

Bernd Ponick
Institute for Drive Systems and Power Electronics
Leibniz Universität Hannover
Ponick@ial.uni-hannover.de
Hannover, Germany

Joerg R. Seume
Institute of Turbomachinery and Fluid Dynamics
Leibniz Universität Hannover
Seume@tfd.uni-hannover.de
Hannover, Germany

ABSTRACT

This paper gives an overview of the interdisciplinary design process of an electrically-powered high-lift system for future commercial aircraft, with a focus on the mixed-flow compressor performance. Based on the requirements of the high-lift system, a multi-objective optimization is used for the aero-mechanical design of the compressor stage. The demand for high pressure ratio and efficiency, together with the constrained installation space yields an unconventional mixed-flow compressor design with a transonic flow regime. To supply the required pressurized air for the high-lift system, rotational speeds of up to 60,000 rpm are necessary according to CFD analysis. A very compact integrated prototype of the compressor system is designed, including electrical machine and power electronics with high power-to-mass ratios. Performance predictions are validated at part load. To integrate the compressor stage into the prototype, some adjustments to the geometry become necessary. Additional CFD simulations reveal a big impact of the new inlet duct on the compressor performance due to inlet flow distortion. It is assumed that a fully-integrated design process, which includes all relevant interdependencies of the different components, would yield a better overall system design.

INTRODUCTION

New technologies are required in order to cope with both increasing passenger numbers in aviation, and stronger regulations regarding noise and greenhouse gases. Due to its beneficial impact on both aircraft performance and noise generation, the high-lift system has great potential to contribute to a solution to these otherwise often conflicting targets. Together with a novel flexible leading-edge device, a combination of boundary layer suction and blowing over a Coanda-surface at the flap is utilized to generate high-lift in an efficient manner during take-off, approach and landing of the aircraft (Radespiel and Heinze, 2014).

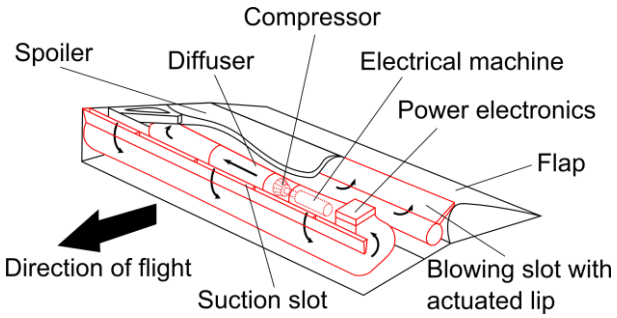

Figure 1 EPHLS Concept (Kauth et al., 2017b)

Instead of burdening the aircraft engine with ancillary functions, the required air for the active high-lift system can be provided by compact, electrically-driven compressor systems (Teichel et al., 2015; Kauth et al., 2017a). By utilizing a boundary layer suction slot on the suction side of the airfoil as intake for the compressor, the efficiency of the active high-lift system can be improved significantly (Burnazzi and Radespiel, 2015; Radespiel et al., 2016). A sketch of this

concept for an electrically-powered high-lift system (EPHLS), which is integrated into the aircraft wing, is presented in Figure 1 (Kauth et al., 2017b). Moreover, this EPHLS offers new potential synergies for prospective 'More Electric Aircraft' concepts (Müller et al., 2018).

METHODOLOGY

The final goal is to develop a multi-disciplinary, integrated design process for the main components of the EPHLS. For this purpose, a multi-objective optimization of the direct and indirect power consumption of the EPHLS is needed which satisfies the constraints of the aircraft application. Direct power consumption means the required electrical power to operate the system, which has to be provided e.g. by generators. Indirect power consumption describes the additional power required from the aircraft engines if the take-off weight is increased. For this reason, both the efficiency and the specific power of the system are target parameters for the optimization.

The core components of the EPHLS are the compressor, the electrical machine, and the power electronics. As a first step towards the goal of a fully integrated, optimized design process for the EPHLS, a reference prototype is designed and evaluated. The components of this prototype are designed using advanced state-of-the-art methods. The air mass flow and pressure ratio to be provided by the compressor are deduced from the jet momentum coefficient required for the blowing at a certain flap angle (Burnazzi and Radespiel, 2015).

$$c_\mu = \frac{\dot{m}_{jet} v_{jet}}{0.5 \rho_\infty {v_\infty}^2 S_{ref}} \qquad (1)$$

These design objectives, together with a constraint for the maximum stage diameter, are input parameters for a newly-developed compressor design process using automatic optimization (Teichel et al., 2017). It yields the shaft power and rotational speed, which are the main parameters to determine the electrical machine design (Narjes et al., 2016). The type of electrical machine and its predicted efficiency are additional parameters required to design the power electronics (Müller and Mertens, 2017).

In parallel, the integrated prototype concept is developed, and the components are adapted to the mechanical requirements of the prototype (Kauth et al., 2017b). Before the integrated prototype is assembled, each component is evaluated experimentally to validate the design methods independently from the other components. The combined, transient operation of the whole system at design speed will be evaluated using the integrated prototype as soon as it becomes available. In the meantime, the compressor has been tested and the performance predictions validated up to 30,000 rpm (aerodynamic design point 60,000 rpm). With the results of the described design process and those of the experimental validation, simplified models for the specific power of each component in dependence of global parameters such as the rotational speed will be derived. These meta-models will then be integrated into a new EPHLS design process, which is assumed to be able to yield a superior global design optimum.

RESULTS AND DISCUSSION

Compressor Design

The aero-mechanical compressor design and optimization process features a differential evolutionary algorithm. First, a parameterized model of the meridional flow path and the rotor blade with 31 degrees of freedom is optimized. Design candidates are evaluated directly by means of Computational Fluid Dynamics (CFD) to find Pareto optimal designs with respect to efficiency and pressure ratio. A stress analysis of each blade design is done using Computational Structural Mechanics to exclude unfeasible designs. After a basic rotor design is chosen, a parameterized blade model of the stator is added and the full stage with 27 degrees of freedom is optimized. The optimization yields an unconventional compressor design with a transonic flow regime. Some important geometrical design parameters are given in Table 1. Figure 2 shows the meridional flow path of the compressor stage. Its significant radius slope characterizes it as a mixed-flow rather than an axial compressor stage. These design features allow high pressure build-up with high efficiency in a single stage (Teichel et al., 2017).

Table 1 Compressor design parameters (Teichel et al., 2017)

Rotor	Blade number	9
	Aspect ratio	0.3
	Solidity	2.0
	Hub-to-tip ratio (inlet)	0.56
Stator	Blade number	11
	Aspect ratio	0.25
	Solidity	1.4
	Hub-to-tip ratio (outlet)	0.85

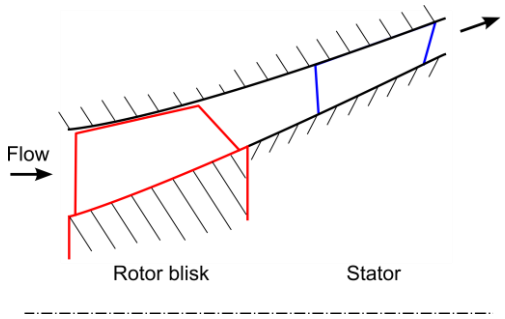

Figure 2 Compressor meridional flow path

Rotational speeds of up to 60,000 rpm are necessary to reach the operating points required for the EPHLS at the most challenging conditions, i.e. high pressure ratio and high mass flow rate at extreme ambient conditions (Teichel et al., 2017). Blisk (blade-integrated disk) geometries are chosen for both rotor and stator due to the compact and highly-loaded stage design. The blisks are machined from a high-strength aluminium alloy to resist the high structural stresses, and to minimize the component's mass (Kauth et al., 2016, Kauth et

al., 2017b). Figure 3 shows the manufactured compressor stage during the assembling for the part-speed experiments.

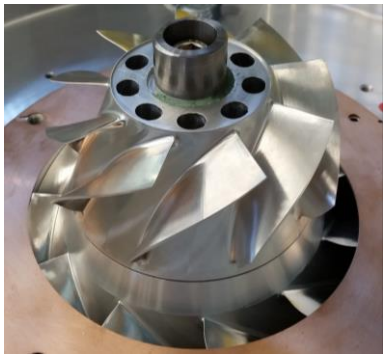

Figure 3 Compressor Stage

Electrical Machine Design

As the EPHLS is only in use during aircraft take-off, approach and landing, the electrical components are designed for transient operation only. This allows using the compressor intake air as a coolant, thus omitting a heavy and bulky liquid cooling system. The maximum operation time of the system is 300 s, which is sufficient for a touch-and-go manoeuvre.

To drive the compressor with the required speed of up to 60,000 rpm, a permanent magnet synchronous machine (PMSM) is designed with a maximum power output of 80 kW. The design of the PMSM requires an interdisciplinary approach. Apart from electromagnetic aspects, the mechanical assessment of the rotor and the thermal evaluation are important. For example, if the rotor geometry is changed due to mechanical stress, this also has an impact on the thermal conditions, the rotor dynamics, and the power output. To resist the high centrifugal forces, carbon fibre is chosen as material for the rotor armour (Narjes et al., 2016). Some of the main design parameters of the PMSM are given in Table 2 (Kauth et al., 2017b).

Table 2 Electrical machine design parameters (Kauth et al., 2017b)

Outer diameter	128 mm
Bore diameter	61 mm
Length of active parts	110 mm
Number of poles	2
Max. power output	80 kW
Max. rotational speed	60,000 rpm

A thermal evaluation model for the electrical machine is implemented in Matlab/Simulink. It consists of a 2D-lumped-parameter-model of the machine's cross section, which is modified to account for axial thermal fluxes. The boundary conditions of the aircraft include a maximum ambient temperature of 50 °C. In the analysis, this temperature is chosen as initial temperature for the components, and as intake temperature of the air. Even for this worst case scenario, the machine can be operated for 300 s without reaching the critical winding temperature of 180 °C. The limiting component is the winding insulation material with thermal class 180 according to IEC 60085 (Narjes et al., 2016).

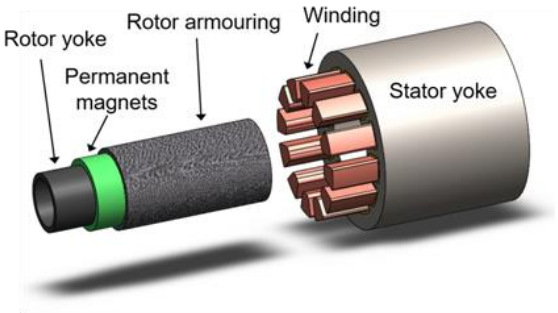

Figure 4 Electrical machine (Kauth et al., 2017b)

The resulting PMSM design is presented in Figure 4. Due to the very compact machine design, a power-to-mass ratio of 7 kW/kg for the active components is achieved (Kauth et al., 2017b). Figure 5 shows the manufactured PMSM rotor.

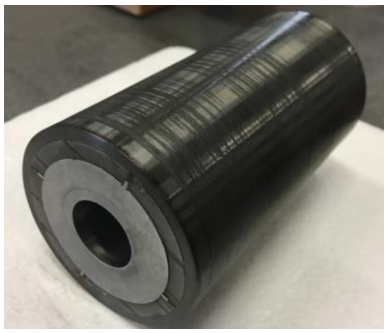

Figure 5 Rotor of Electrical Machine

Power Electronics Design

The voltage source inverter (VSI) is designed using an innovative three-dimensional power module and DC-link interconnection to cope with the restricted spatial conditions in combination with forced convection and high switching speed of the silicon carbide field effect transistors (SiC-MOSFETs). The power loss estimation is evaluated by switching tests to derive an accurate loss model. Additionally, a heat-sink optimization process is performed using analytical calculations as well as CFD simulations. To validate the approach, thermal measurements are performed. For this purpose, the power modules are heated through on-state power dissipation for the rated conditions of the final system (Kauth et al., 2017b; Müller and Mertens, 2017).

The gate driver offers under-voltage as well as over-current protection. Furthermore, the isolated DC/DC converter allows switching frequencies of up to 64 kHz. In addition, a brake chopper is integrated which is activated as soon as a voltage of 900 V is exceeded in the case of braking operation of the PMSM at high speed. For the transmission of the switching as well as status signals, 9 channels of optical fibres are installed.

The SiC MOSFET half-bridge modules are mounted on an annular heat sink, which is integrated into the intake duct of the compressor upstream of the electrical machine (see Figure 7). This arrangement is necessary, as the power electronics need to be designed for steady-state operation due to small thermal time constants, thereby requiring the lowest

coolant temperature possible. Due to the high switching speed of SiC, the inductance of the commutation loops must be minimized (Mueller and Bayerer, 2014). Therefore, an eight-level Power printed circuit board (PCB) is designed. First, the PCB is soldered and the basic functionality is tested. Then, the three-dimensional structure is achieved by bending the PCB by an angle of 90° at the milled slots. Figure 6 shows the manufactured final design (Kauth et al., 2017b).

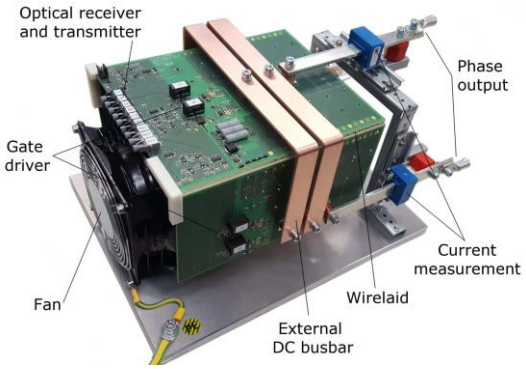

Figure 6 Power Electronics (Kauth et al., 2017b)

Integrated Prototype Design

Both the restriction of available space and the goal of minimized mass demand a highly integrated prototype design. For the bearing system, high-speed precision ball-bearings with grease lubrication are chosen to make an additional oil-cycle obsolete. Duplex angular contact ball bearings in a tandem arrangement are used to resist the combined axial and radial loads of the compressor. A reduction of the axial forces is necessary to increase the lifetime of the bearings. This is achieved through a connection of the upstream and downstream blisk cavities (Kauth et al., 2017b).

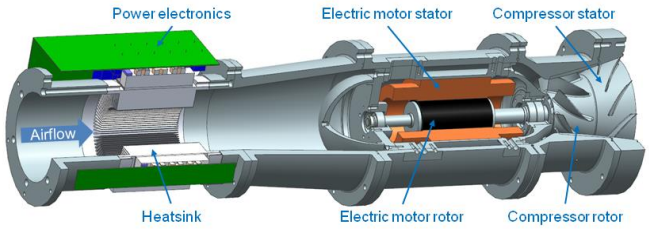

Figure 7 Integrated Prototype (Kauth et al., 2017b)

During the mechanical design of the integrated prototype, some adjustments have to be done to the optimized compressor stage geometry. To allow their manufacture by milling, leading edge (LE) and trailing edge (TE) radius of the compressor blades were increased to a minimum of 0.25 mm (Kauth et al., 2017b). An initial concept of placing the compressor upstream of the motor has to be discarded, as the compressed air at the compressor outlet is too hot to maintain sufficient cooling of the electrical machine. Additionally, the shaft has to be as short as possible to limit the radial displacement when critical rotor speeds are passed. This leads to a relatively sharp flow turning at the compressor inlet, which was not part of the compressor stage model used during the optimization. Figure 7 shows the final design of the integrated prototype (Kauth et al., 2017b).

Compressor Performance Evaluation

The part-speed performance of the compressor was validated using a commercial electric motor with a maximum rotational speed of 30,000 rpm (Kauth et al., 2017b). Two experimentally determined performance curves are shown in Figure 8 in comparison with the CFD predictions. Error bars indicating the 90 % confidence interval (CI) are mostly within the symbol size. The numerical model used in this case has been adapted to the flow path of the test facility, which differs from the one of the integrated prototype. Measured pressure ratios match the CFD predictions within 1 %. Stall inception was observed at up to 7 % lower mass flow rates compared to the last converged CFD simulation at a particular rotational speed. Experimentally determined efficiencies (see Figure 9) are up to 3 % lower compared to the CFD predictions. The reason for this difference is not fully understood yet and subject to ongoing investigations. The experiments did not include any transonic operating points of the compressor, further testing with the newly developed electrical machine is still necessary.

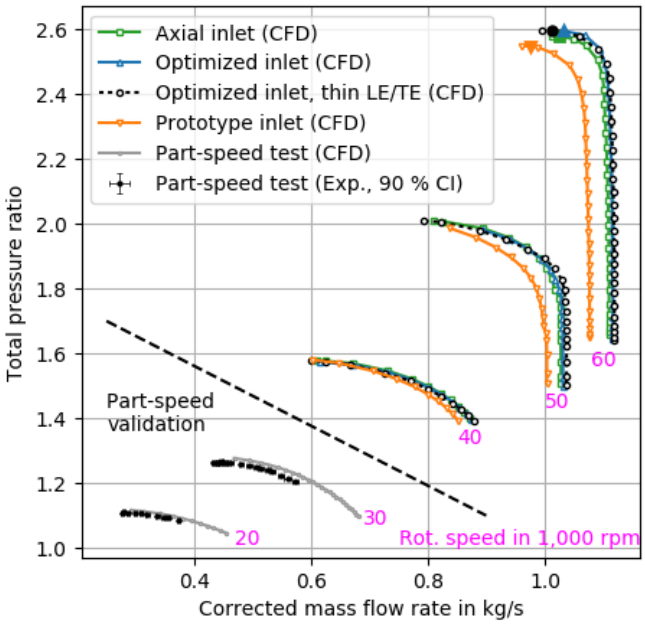

Figure 8 Performance maps of compressor stage variations (experimental data shown with 90 % confidence intervals)

As long as the integrated prototype is not available, the compressor performance at higher rotational speed can only be evaluated by means of CFD. The industrial CFD code TRACE (Deutsches Zentrum für Luft- und Raumfahrt, 2017; Kügeler et al., 2008) is used for the CFD simulations. The governing equations are discretized using the finite volume method. Time discretization is done by means of an implicit first-order Euler method and a predictor-corrector algorithm is applied by the solver. Fully-turbulent flow is assumed and turbulence is modelled using the two-equation k-ω model

(Wilcox, 1988), which is extended to fix the stagnation point anomaly, and to model compressible and rotational effects (Röber et al., 2006). Walls are treated as adiabatic with a non-slip condition. Due to the low-Reynolds number approach, all meshes are generated with a dimensionless wall-distance near one. Boundary conditions imposed at the inlet are total pressure of 101350 Pa, total temperature of 288.15 K, turbulent intensity of 5 %, and turbulent length scale of 18.8 µm. At the outlet, an average static pressure is imposed, which is varied to compute the performance curves. The interfaces between rotating and stationary domains are modelled using mixing-planes.

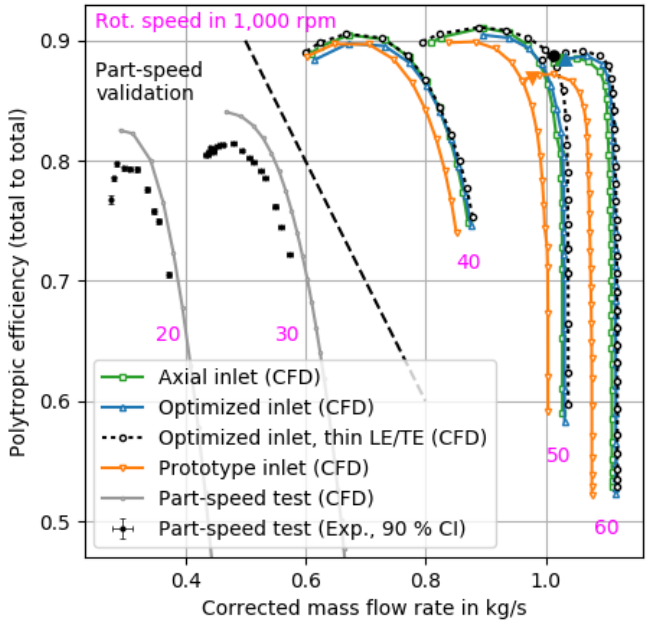

Figure 9 Polytropic efficiencies of compressor stage variations (experimental data shown with 90 % confidence intervals)

First, the influence of the thicker edges of the manufactured blades on the compressor performance is analysed. For this purpose, new meshes for the rotor and stator blades with the thicker LE and TE are generated using a similar topology and resolution as for the original optimized blades. It is expected that the curved inlet duct of the integrated prototype leads to compressor inlet flow distortion, which can have a big impact on the compressor performance (Cumpsty, 2004). To assess the influence of different inlet geometries, additional meshes are generated for the 'prototype inlet' duct and an 'axial inlet' duct. The inlet duct from the original stage design is referred to as 'optimized inlet'. Compressor performance is computed by means of CFD at rotational speeds between 40,000 and 60,000 rpm. The resulting performance curves are presented in Figure 8. The mass flow rate is corrected using the reference pressure p_{ref} = 101325 Pa and the reference temperature T_{ref} = 288.15 K (international standard atmosphere).

$$\dot{m}_{corr} = \dot{m}\frac{p_{ref}}{p}\sqrt{\frac{T}{T_{ref}}} \qquad (2)$$

The corresponding polytropic efficiencies are presented in Figure 9.

$$\eta_p = \frac{\kappa-1}{\kappa}\frac{\ln(PR_{tt})}{\ln(TR_{tt})} \qquad (3)$$

According to the simulation results, the effect of the thicker blade LE and TE is very small, even at the transonic operating points of the compressor. The thicker blade edges seem to have no significant effect on the pressure ratio, while the maximum mass flow rate and peak efficiency are slightly reduced.

Table 3: Peak performance points of compressor stage variations

Case	Corrected mass flow rate in kg/s	Total pressure ratio	Polytropic efficiency in %
Optimized inlet, thin LE/TE	1.01	2.60	88.7
Optimized inlet	1.03	2.60	88.4
Axial inlet	1.02	2.58	88.4
Prototype inlet	0.98	2.55	87.0

Both the maximum pressure ratio and the mass flow rate are reduced by the alternative inlet ducts. Particularly the prototype inlet severely affects the performance. Table 3 summarizes the most important performance parameters for the operating points with the highest total pressure ratio ('peak performance') at maximum rotational speed, i.e. 60,000 rpm. These operating points are also highlighted by larger, filled symbols in Figure 8 and Figure 9.

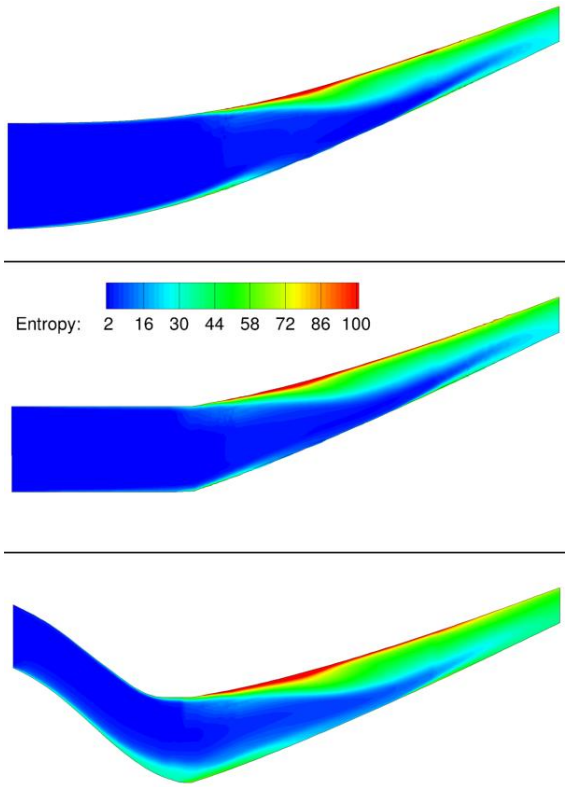

Figure 10 Meridional distributions of entropy (in J/K) in compressor stage (top: optimized inlet, middle: axial inlet, bottom: prototype inlet)

In Figure 10 the circumferentially mass-averaged entropy distributions are presented for the different inlet ducts at the peak performance points. Compared to the other geometries, higher losses are introduced already in the prototype inlet duct due to its curved shape.

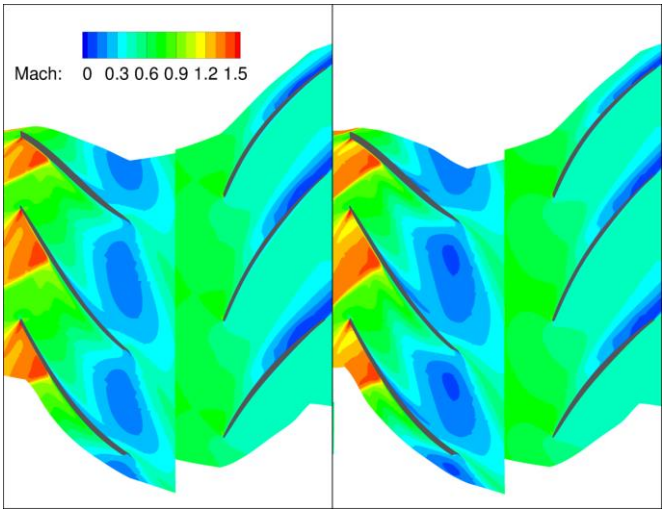

Figure 11 Relative Mach number distribution near shroud (left: optimized inlet, right: prototype inlet)

Figure 11 shows the relative Mach number distributions at 90 % span for the optimized inlet and the prototype inlet at the same operating points as discussed before. The flow distortion introduced by the prototype inlet duct leads to higher Mach numbers along the suction side of the rotor profile and ultimately to a stronger shock with higher losses. As a consequence, the area of the secondary flow region at the rotor exit is increased.

CONCLUSIONS

In this paper, it is demonstrated that by employing state-of-the-art methods and novel design concepts such as optimization during the design of the components of an electrically powered high-lift system, a very compact and efficient compression system can be achieved which meets all design requirements. Experimental validation of the numerical models applied in the design process is achieved at part-speed. Full-speed validation is forthcoming.

However, the mostly sequential design process is not only time consuming, but also leads to some design choices which are not optimal. For instance, the final adjustments to the compressor inlet duct due to the thermal requirements of the electrical machine and the mechanical prototype design have a high impact on the compressor performance, according to the new CFD simulations.

For exceeding the design requirements, a fully integrated design process must include all relevant interdisciplinary interdependencies of the different components. The next important steps therefore are the experimental validation of the design methods and the numerical predictions at full-speed using the newly designed integrated prototype, followed by a fully integrated optimization study including flow, stresses, and cooling of the power electronics, the electrical machine, and the transonic mixed-flow compressor.

NOMENCLATURE

S_{ref}	Reference surface
PR_{tt}	Total pressure ratio
TR_{tt}	Total temperature ratio
c_μ	Jet momentum coefficient
$\dot{m}$	Mass flow rate
p	Pressure
v_{ref}	Reference velocity
v_∞	Free stream velocity
η_p	Polytropic efficiency
κ	Heat capacity ratio
ρ	Density

ACKNOWLEDGMENTS

The authors would like to thank the German Research Foundation (DFG) for supporting this fundamental research in active high-lift systems for future aircraft as part of the Collaborative Research Centre 880 (Sonderforschungsbereich SFB 880). Moreover, the authors thank the German Aerospace Center (DLR) for the permission to use the solver TRACE, and Raffael Thiessen for his support.

REFERENCES

Burnazzi, M., Radespiel, R. (2015). Synergies between suction and blowing for active high-lift flaps. CEAS Aeronautical Journal 6, 305–318. doi:10.1007/s13272-014-0146-8.

Cumpsty, N.A. (2004). Compressor aerodynamics, 2nd ed., Malabar, Florida: Krieger Publishing.

Deutsches Zentrum für Luft- und Raumfahrt (2017). TRACE User Guide (December 2017). http://www.trace-portal.de/userguide/trace/index.html.

International Electrotechnical Commission (2007). IEC 60085:2007: Electrical Insulation – Thermal Evaluation and Designation.

Kauth, F., Narjes, G., Müller, J., Mertens, A., Ponick, B., and Seume, J.R. (2016). Highly Integrated Electrically Driven Active High-Lift Compressor Systems for Future Civil Aircraft. In: Greener Aviation Conference, Brussels, Belgium.

Kauth, F., Narjes, G., Müller, J., Seume, J.R., Vasista, S., Müller, T., Francois, D.G., El Sayed M., Y., Semaan, R., Behr, C., Schwerter, M., Leester-Schädel, M., Nolte, F., Giesecke, D., Atalayer, C., Radespiel, R. (2017a). Progress in Efficient Active High-Lift. In: 35th AIAA Applied Aerodynamics Conference. Denver, Colorado. doi:10.2514/6.2017-3559.

Kauth, F., Narjes, G., Müller, J., Ponick, B., Mertens, A., Seume, J.R. (2017b). Compact Electrical Compressors for Active Flow Control in Autonomous High-Lift Systems. In: SFB 880 - Fundamentals of High-Lift for Future Civil Aircraft: Biennial Report, ed. Radespiel, R., Semaan, R. Braunschweig: Campus Forschungsflughafen, 105-116.

Kügeler, E., Nürnberger, D., Weber, A., Engel, K. (2008). Influence of blade fillets on the performance of a 15 stage gas

turbine compressor. In: Proccedings of ASME Turbo Expo. doi:10.1115/GT2008-50748.

Mueller, C.R., Bayerer, R. (2014). Low-inductive inverter concept by 200A / 1200V half bridge in an EasyPACK 2B – following strip-line design. In: International Conference on Integrated Power Electronics Systems. Nuremberg, Germany.

Müller, J., Mertens, A. (2017). Power Electronics Design for a Direct-Driven Turbo Compressor Used as Advanced High-Lift System in Future Aircraft. In: 43rd Annual Conference of the IEEE Industrial Electronics Society. Beijing, China.

Mueller, J.-K., Bensmann, A., Bensmann, B., Fischer, T., Kadyk, T., Narjes, G., Kauth, F., Ponick, B., Seume, J., Krewer, U., Hanke-Rauschenbach, R., Mertens, A. (2018). Design Considerations for the Electrical Power Supply of Future Civil Aircraft with Active High-Lift Systems. Energies 11, 179. doi:10.3390/en11010179.

Narjes, G., Müller, J., Mertens, A., Ponick, B., Kauth, F., Seume, J.R. (2016). Design Considerations for an Electrical Machine Propelling a Direct Driven Turbo Compressor for Use in Active High-Lift Systems. In: ESARS-ITEC Conference, Toulouse, France. doi:10.1109/ESARS-ITEC.2016.7841338.

Radespiel, R., Heinze, W. (2014). SFB 880: fundamentals of high lift for future commercial aircraft. CEAS Aeronautical Journal 5, 239–251. doi:10.1007/s13272-014-0103-6.

Radespiel, R., Burnazzi, M., Casper, M., Scholz, P. (2016). Active Flow Control for High Lift with Steady Blowing. The Aeronautical Journal 120, 171–200. doi:10.1017/aer.2015.7

Röber, T., Kožulović, D., Kügeler, E., Nürnberger, D. (2006). Appropriate turbulence modelling for turbomachinery flows using a two-equation turbulence model. In: New Results in Numerical and Experimental Fluid Mechanics V. Springer, Berlin, Heidelberg, pp. 446–454. doi:10.1007/978-3-540-33287-9_55.

Teichel, S.H., Dörbaum, M., Misir, O., Merkert, A., Mertens, A., Seume, J.R., Ponick, B. (2015). Design Considerations for the Components of Electrically Powered Active High-lift Systems in Civil Aircraft. CEAS Aeronautical Journal 6, 49–67. doi:10.1007/s13272-014-0124-1.

Teichel, S.H., Verstraete, T., Seume, J.R. (2017). Optimized Multidisciplinary Design of a Small Transonic Compressor for Active High-Lift Systems. International Journal of Gas Turbine, Propulsion and Power Systems 9, 19–26.

Wilcox, D.C. (1988). Reassessment of the scale-determining equation for advanced turbulence models. AIAA Journal 26, 1299–1310. doi:/10.2514/3.10041.